

# Geophysical Research Letters



## RESEARCH LETTER

10.1029/2021GL092836

### Key Points:

- H<sub>2</sub>O solubility in Fe-bearing wadsleyite decreases with increasing temperature
- Fe-bearing wadsleyite can contain ~1.0 wt.% H<sub>2</sub>O at mantle transition zone temperature
- Dehydration melting could occur at the 520-km discontinuity by upwelling flow near plumes

### Supporting Information:

Supporting Information may be found in the online version of this article.

### Correspondence to:

H. Fei,  
[hongzhan.fe@uni-bayreuth.de](mailto:hongzhan.fe@uni-bayreuth.de)

### Citation:

Fei, H., & Katsura, T. (2021). Water solubility in Fe-bearing wadsleyite at mantle transition zone temperatures. *Geophysical Research Letters*, *48*, e2021GL092836. <https://doi.org/10.1029/2021GL092836>

Received 7 FEB 2021  
 Accepted 5 APR 2021

## Water Solubility in Fe-Bearing Wadsleyite at Mantle Transition Zone Temperatures

Hongzhan Fei<sup>1</sup>  and Tomoo Katsura<sup>1,2</sup> 

HPSTAR  
 1220-2021

<sup>1</sup>Bayerisches Geoinstitut, Universität Bayreuth, Bayreuth, Germany, <sup>2</sup>Center for High Pressure Science and Technology Advanced Research, Beijing, P.R. China

**Abstract** Wadsleyite can store significant amounts of H<sub>2</sub>O in its crystal structure as hydroxyl. However, H<sub>2</sub>O solubility in Fe-bearing wadsleyite remains poorly constrained at mantle transition zone temperatures. Previous studies (e.g., Demouchy et al., 2005 [<https://doi.org/10.2138/am.2005.1751>]; Litasov et al., 2011 [<https://doi.org/10.1007/s00269-010-0382-3>]) focused primarily on Fe-free systems, which do not represent the Earth's interior because Fe may affect the H<sub>2</sub>O solubility. Here, we investigated the temperature dependence of H<sub>2</sub>O solubility in Fe-bearing and Fe-free wadsleyite at 1500–2100 K. The results indicate that H<sub>2</sub>O solubility in Fe-bearing wadsleyite is higher than in Fe-free samples at 1800–1900 K, corresponding to transition zone geotherm, but there is no clear Fe content dependence in the Fe-bearing samples. Wadsleyite can contain approximately 1.0 wt.% H<sub>2</sub>O at transition zone temperatures. The H<sub>2</sub>O solubility in wadsleyite is lower than ringwoodite along a plume geotherm, which may result in dehydration melting at the 520-km discontinuity by upwelling flow in plumes.

**Plain Language Summary** The mantle transition zone at 410–660 km depth is a H<sub>2</sub>O sponge because wadsleyite and ringwoodite can contain large amounts of H<sub>2</sub>O in their crystal structures as hydroxyl defects. However, the solubility of H<sub>2</sub>O in Fe-bearing wadsleyite is poorly constrained compared with ringwoodite and Fe-free wadsleyite, which have been extensively investigated. The exact H<sub>2</sub>O storage capacity of the mantle transition zone, therefore, remains unknown. Here, we investigated the solubility of H<sub>2</sub>O in Fe-bearing wadsleyite as a function of temperature. The results indicate that wadsleyite can store ~1.0 wt.% H<sub>2</sub>O at transition zone temperatures and ~0.65 wt.% along a plume geotherm. H<sub>2</sub>O solubility in wadsleyite is lower than that in ringwoodite in mantle plumes. A dehydration melting layer at the 520-km discontinuity near plumes can, therefore, form via the phase transition from ringwoodite to wadsleyite under H<sub>2</sub>O-saturated conditions driven by upwelling flow in mantle plumes.

## 1. Introduction

Wadsleyite, with a chemical formula of (Mg,Fe)<sub>2</sub>SiO<sub>4</sub>, is the dominant mineral in the upper part of the mantle transition zone from 410 to 520 km depth. Because wadsleyite can contain up to ~3.0 wt.% H<sub>2</sub>O as hydroxyl in its crystal structure (Kohlstedt et al., 1996; Smyth et al., 1987, 1994), the transition zone is considered to be a sponge in the Earth's interior. The presence of H<sub>2</sub>O can significantly affect the physical and chemical properties of wadsleyite, including atomic diffusivity, electrical conductivity, phase transition, elasticity, and rheology (Buchen et al., 2018; Chen et al., 2002; Dai & Karato, 2009; Demouchy et al., 2011; Manthilake et al., 2009; Shimajuku et al., 2010; Yoshino et al., 2008; Yoshino & Katsura, 2013; Zhang et al., 2021; Zhang & Xia, 2021), thus, information regarding H<sub>2</sub>O incorporation in wadsleyite is essential for understanding mantle dynamics. Because H<sub>2</sub>O-rich fluid and silicate melt are miscible at high pressure, the H<sub>2</sub>O solubility (storage capacity) in high-pressure minerals is defined as the maximum amount of H<sub>2</sub>O that can be dissolved in a crystal coexisting with hydrous silicate melt under a given pressure and temperature conditions (Demouchy et al., 2005; Hirschmann et al., 2005). The solubility of H<sub>2</sub>O in wadsleyite therefore represents the maximum possible amount of H<sub>2</sub>O in the upper part of the mantle transition zone.

Despite of its importance, however, the question of H<sub>2</sub>O solubility in wadsleyite remains unsolved. Although H<sub>2</sub>O solubility has been extensively studied in the Fe-free wadsleyite endmember (Demouchy et al., 2005; Druzhbin et al., 2021; Litasov et al., 2011; Zhu et al., 2019), that in the Fe-bearing system remains poorly constrained. Sun et al. (2018) reported the H<sub>2</sub>O content (C<sub>H2O</sub>) of approximately 1.0 wt.% in Fe-bearing wadsleyite synthesized at 1720 K under H<sub>2</sub>O-saturated conditions, which is more than twice that reported

© 2021. The Authors.

This is an open access article under the terms of the [Creative Commons Attribution License](https://creativecommons.org/licenses/by/4.0/), which permits use, distribution and reproduction in any medium, provided the original work is properly cited.

**Table 1**

List of Run Conditions, Phases in the Run Products, Thicknesses for FTIR Analysis,  $C_{H_2O}$ ,  $(Mg + Fe)/Si$ , and  $Fe/(Mg + Fe)$  Ratios in Wadsleyite

Starting material <sup>a</sup>	Run no.	P (GPa)	T (K)	Duration (min)	Phases	(Mg + Fe)/Si ratio	Fe/(Mg + Fe) ratio	Thickness ( $\mu$ m)	Number of spectra	$C_{H_2O}$ (wt.%)
Fo90 + 15% $H_2O$	S7114Ol	17.5	2100	30	Wds + melt	1.990 (17)	4.18 (9) %	20	5	0.65 (10)
	H4817Ol	17.5	1700	300	Wds + En?+melt	1.916 (19)	5.65 (14) %	21	6	1.34 (22)
								12	6	1.36 (29)
	H4898Ol	17.5	1500	300	Wds + PhB + melt	1.840 (14)	6.60 (43) %	22	5	2.14 (29)
								12	6	2.20 (45)
H4841Ol	17.5	1900	120	Wds + melt	1.952 (18)	5.08 (9) %	19	5	1.03 (16)	
								12	6	1.01 (20)
Fo75 + 15% $H_2O$	H4821Ol	17.5	1900	120	Wds + En + melt	1.946 (13)	12.35 (91) %	21	5	0.94 (16)
Fo100 + 15% $H_2O$	H4821Fo	17.5	1900	120	Wds + En + melt	1.941 (15)	0.04 (3) %	21	5	0.73 (12)
								12	6	2.42 (52)
Fo100 + 5% $H_2O$	H4790Fo	21	2000	300	Wds + En + melt	1.961 (14)	0.03 (3) %	20	6	0.58 (10)

Abbreviations: En, high pressure phase of enstatite; FTIR, Fourier transformation infrared spectroscopy; P, pressure; PhB: superhydrous phase B; T, temperature; Wds, wadsleyite.

<sup>a</sup>Starting material is a mixture MgO, SiO<sub>2</sub>, FeO, and Mg(OH)<sub>2</sub> with a bulk composition of (Mg<sub>1.8</sub>Fe<sub>0.2</sub>)SiO<sub>4</sub> (Fo90), (Mg<sub>1.5</sub>Fe<sub>0.5</sub>)SiO<sub>4</sub> (Fo75), or Mg<sub>2</sub>SiO<sub>4</sub> (Fo100) + 15% or 5% H<sub>2</sub>O. The weight ratio of the silicate and H<sub>2</sub>O is 100:15 or 100:5. Namely, the bulk  $C_{H_2O}$  content is 4.76 wt.% [=5/(100 + 5)] or 13.04 wt.% [=15/(100 + 15)].

by Bolfan-Casanova et al. (2018) under comparable conditions. Kohlstedt et al. (1996) reported a H<sub>2</sub>O solubility of 2.1–2.4 wt.% in Fe-bearing wadsleyite, but their experiments were performed at 1370 K, substantially lower than transition zone temperatures (1800–1900 K at 410–520 km depth Katsura et al., 2010). By considering the temperature dependence of H<sub>2</sub>O solubility in minerals (Demouchy et al., 2005; Litasov et al., 2011) and possible Fe effect on H<sub>2</sub>O incorporation, a systematic study regarding H<sub>2</sub>O solubility in Fe-bearing wadsleyite is required to understand the H<sub>2</sub>O incorporation and storage capacity in the mantle transition zone.

In this study, we measured H<sub>2</sub>O solubility in Fe-bearing wadsleyite at 17.5 and 21 GPa as a function of temperature from 1500 to 2100 K, which covers the entire temperature range for wadsleyite in the Earth's interior from cold slabs to hot spots. H<sub>2</sub>O solubility in Fe-free wadsleyite was also investigated for comparison. Note that oxygen fugacity ( $f_{O_2}$ ) may affect H<sub>2</sub>O solubility in upper mantle minerals (Liu & Yang, 2020; Yang, 2016). However, as we investigated recently (Druzhbin et al., 2021), H<sub>2</sub>O solubility in Fe-free wadsleyite is independent from  $f_{O_2}$ . It should be also the case for Fe-bearing wadsleyite because dissociation of H<sub>2</sub>O is negligible under transition zone conditions (Druzhbin et al., 2021). This is proved by the positive correlation between  $Fe^{3+}/\Sigma Fe$  and  $f_{O_2}$ , but no correlation between  $Fe^{3+}/\Sigma Fe$  and H<sub>2</sub>O-solubility (McCammon et al., 2004; Mrosko et al., 2013); with increasing  $Fe^{3+}/\Sigma Fe$  from 28% to 96%, the H<sub>2</sub>O-solubility in wadsleyite does not show any variation (McCammon et al., 2004). Therefore, the  $f_{O_2}$  in this study is self-buffered by the samples without additional buffering materials.

## 2. Experimental and Analytical Methods

### 2.1. Starting Material and High-Pressure Experiments

MgO, SiO<sub>2</sub>, FeO, and Mg(OH)<sub>2</sub> (purities >99.99%) were used as the starting materials. The MgO and SiO<sub>2</sub> were dried at 1370 K in an ambient-pressure furnace, whereas FeO and Mg(OH)<sub>2</sub> were dried at 400 K in a vacuum furnace prior to weighing. Mixtures with a bulk composition of Mg<sub>2</sub>SiO<sub>4</sub> and (Mg,Fe)<sub>2</sub>SiO<sub>4</sub> + 5 or 15 wt.% H<sub>2</sub>O (Table 1) were prepared by grinding in ethanol using an agate mortar. The powders were stored in a vacuum furnace at 400 K prior to use (Fei & Katsura, 2020).

High-pressure experiments were performed using the multi-anvil technique. To reduce the amount of Fe absorbed by the sample capsule, Pt-Rh capsules were used. The Fe-content should be within 2.0 wt.% in a 1 ~ 2- $\mu\text{m}$  layer on the inner wall of the capsule and less than 0.2 wt.% at 6  $\mu\text{m}$  away from the wall (Fei & Katsura, 2020), which is negligible in comparison with the total amount of Fe in the samples. The starting materials were welded in Pt-Rh capsules with inner diameter of 1.0 mm, outer diameter of 1.2 mm, and length of 1.0–1.3 mm. One or two capsules were loaded into an MgO sleeve in each multi-anvil cell assembly with a LaCrO<sub>3</sub> heater, ZrO<sub>2</sub> thermal insulator, and Cr<sub>2</sub>O<sub>3</sub>-doped MgO octahedron with an edge length of 10 mm. The assembly was compressed to 17.5 or 21 GPa at room temperature using eight tungsten carbide cubes with truncated edge lengths of 5 (for 17.5 GPa runs) or 4 mm (for 21 GPa runs). The temperature was sequentially increased to the desired value using a ramping rate of ~100 K/min measured by a D-type (W/Re) thermocouple and annealed for 30–300 min (Table 1). The assembly was then quenched to ambient temperature by switching off the heating power, and the pressure was reduced to ambient condition over a duration of more than 10 h.

## 2.2. Sample Analysis

Cross sections of the recovered capsules were prepared by polishing with sandpaper and diamond powder. The textures in the cross sections were observed by scanning electron microprobe (SEM) using a backscattering electron detector (BSE) with an acceleration voltage of 15 kV and an energy-dispersive spectrometer (EDS).

The concentrations of MgO, SiO<sub>2</sub>, and FeO in wadsleyite were measured using a JEOL JXA-8200 electron probe microanalyzer (EPMA) with a wavelength-dispersive spectrometer (WDS). A forsterite single crystal was used as the standard for MgO and SiO<sub>2</sub>, and a metallic Fe standard was used for FeO. The acceleration voltage and beam current were 15 kV and 15 nA, respectively, with a counting time of 20 s for each analysis point using a focused beam. The (Mg + Fe)/Si atomic ratios and Fe contents [Fe/(Mg + Fe)] were calculated from the EPMA results (Supporting Information).

The  $C_{\text{H}_2\text{O}}$  in wadsleyite was analyzed by unpolarized Fourier transformation infrared spectroscopy (FTIR) using a Bruker IFS 120 high-resolution spectrometer coupled with a Bruker IR microscope. The sample capsules were double-side polished to a thickness of approximately 20  $\mu\text{m}$  for FTIR analysis. To examine the possible saturation of infrared absorption, some samples were further polished to a thickness of 12  $\mu\text{m}$  (Table 1). One or two hundred scans were accumulated for each FTIR spectrum at a resolution of 2  $\text{cm}^{-1}$ . Crystal boundaries and cracks were avoided. Five or six spectra from multiple grains with random crystallographic orientations were obtained for each sample.

After baseline correction, the  $C_{\text{H}_2\text{O}}$  in wadsleyite was calculated from the Beer–Lambert law,

$$C_{\text{H}_2\text{O}} = 10^6 \times \int \frac{3H(\nu)M_{\text{H}_2\text{O}}}{\epsilon\tau\rho} d\nu \quad (1)$$

where  $C_{\text{H}_2\text{O}}$  is the H<sub>2</sub>O content in wt. ppm,  $\nu$  is the wavenumber,  $H(\nu)$  is the infrared absorption at wavenumber  $\nu$ ,  $M_{\text{H}_2\text{O}}$  is the molar weight of H<sub>2</sub>O (18.02 g/mol),  $\epsilon$  is the absorption coefficient (69,000  $\pm$  7,000 L/(mol  $\text{cm}^2$ ) and 67,000  $\pm$  5,000 L/(mol  $\text{cm}^2$ ) for Fe-free and Fe-bearing wadsleyite, respectively [Bolfan-Casanova et al., 2018]),  $\tau$  is the sample thickness, and  $\rho$  is the density (3,500 g/L [Jacobsen et al., 2005]). The integration is performed in the range of 3,000–4,000  $\text{cm}^{-1}$ . The uncertainty of  $C_{\text{H}_2\text{O}}$  is calculated from the standard deviation from the multiple spectra, uncertainty of  $\epsilon$ , and uncertainty of the thickness measurements ( $\pm 1$   $\mu\text{m}$ ). Note that if using  $\epsilon = 73,000 \pm 7,000$  L/(mol  $\text{cm}^2$ ) reported by Deon et al. (2010), the retrieved  $C_{\text{H}_2\text{O}}$  values are systematically lower by 5%–8% (Table 1).

## 3. Results and Comparison With Previous Studies

### 3.1. Sample Textures

The samples appear as wadsleyite single crystals with grain sizes of 20–500  $\mu\text{m}$  coexisting with or without enstatite [(Mg,Fe)SiO<sub>3</sub> or MgSiO<sub>3</sub>], and quenched crystallized melt as confirmed by SEM and EDS

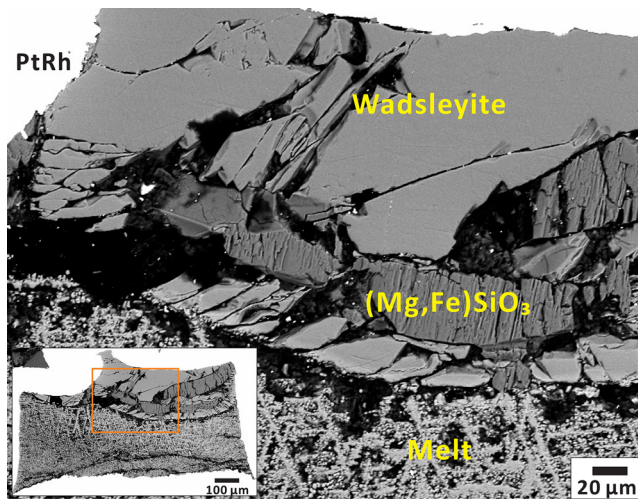


**Figure 1.** BSE image of H4821Ol (Fe-bearing, 1900 K), which appears as a coexistence of wadsleyite, enstatite [(Mg,Fe)SiO<sub>3</sub>], and quenched crystallized melt. BSE, backscattering electron detector.

(Figure 1). Superhydrous phase B appeared instead of enstatite in H4898 likely because of the low temperature stability of the dense hydrous magnesium silicate phase.

Ringwoodite was not observed. This is reasonable because Fe preferably participates into melt (e.g., Fei & Katsura, 2020), as a result, the Fe content in wadsleyite is relatively low ( $\text{Fe}/(\text{Mg} + \text{Fe}) \leq 12.4\%$  [Table 1]), which is within the wadsleyite single-phase stability field under our experimental conditions (Katsura & Ito, 1989; Frost, 2003).

### 3.2. FTIR Spectra

Raw data of FTIR spectra without baseline subtraction and thickness normalization are shown in Figure 2a. The raw data can be directly compared because all of the samples have a comparable thickness (from 19 to 22  $\mu\text{m}$ ). A plateau at 3,300–3,350  $\text{cm}^{-1}$  does not appear, which indicates no infrared absorption saturation (Druzhbin et al., 2021). This is also confirmed by the identical infrared absorbance (identical  $C_{\text{H}_2\text{O}}$ ) between the samples with thickness of 21–22 and 12  $\mu\text{m}$  after thickness normalization (Figure 2b; Table 1).

All of the spectra show sharp peaks at wavenumbers of 3,610, 3,581, 3,355, and 3,325  $\text{cm}^{-1}$ , which agree with previous studies (e.g., Bolfan-Casanova et al., 2018; Deon et al., 2010; Druzhbin et al., 2021; Jacobsen et al., 2005; Litasov et al., 2011; Smyth et al., 2005). The peak at 3,610  $\text{cm}^{-1}$  in the Fe-bearing samples is significant, whereas that in the Fe-free wadsleyite is negligible. In contrast, the 3,581, 3,325, and 3,355  $\text{cm}^{-1}$  peaks are comparable between

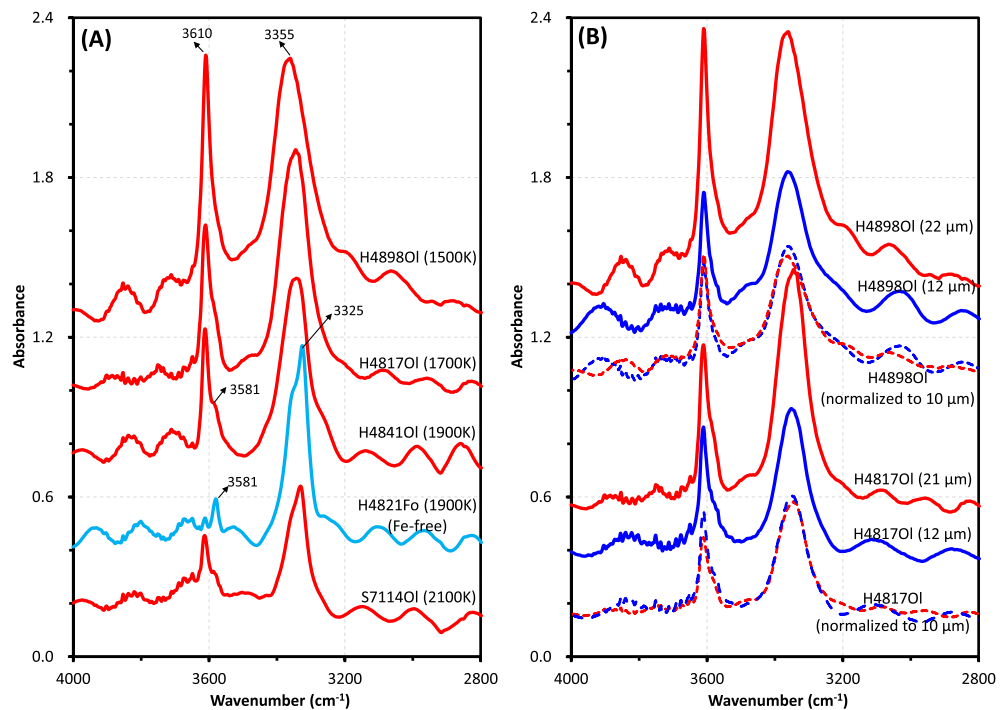


**Figure 2.** Representative unpolarized FTIR spectra obtained in the recovered samples. (a) Spectra at about 20  $\mu\text{m}$  thickness. (b) Spectra of H4898Ol and H4817Ol. The solid red and blue curves denote spectra at thickness of 22 and 12  $\mu\text{m}$ , respectively. The dash curves are after thickness normalization to 10  $\mu\text{m}$ . The agreement of infrared absorbance after thickness normalization indicates no saturation of infrared absorption. All spectra are raw data without baseline subtraction but vertically shifted for visibility. Sinusoid shape wave interference occurs because of the small sample thickness. FTIR, Fourier transformation infrared spectroscopy.

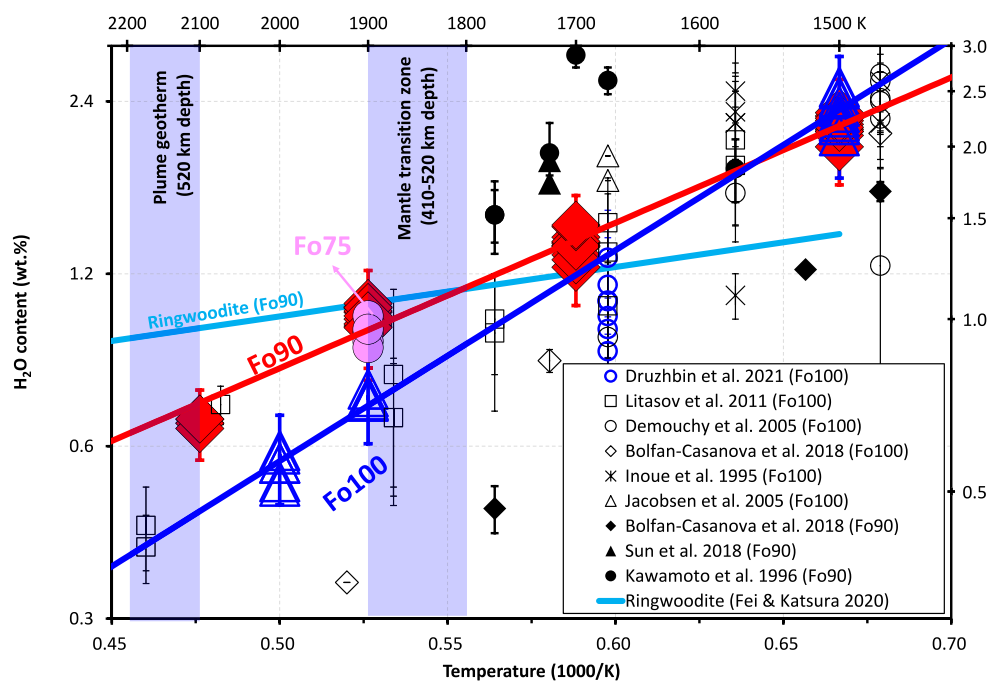


**Figure 3.**  $H_2O$  content/solubility in Fe-bearing (filled symbols) and Fe-free (unfilled symbols) wadsleyite. The Fo100, Fo90, and Fo75 represent the Fe contents in the starting materials of each study corresponding to  $Mg_2SiO_4$ ,  $(Mg_{1.8}Fe_{0.2})SiO_4$ , and  $(Mg_{1.5}Fe_{0.5})SiO_4$ , respectively. Each symbol of this study represents a  $C_{H_2O}$  value from one FTIR spectrum. The  $C_{H_2O}$  from Jacobsen et al. (2005) and Litasov et al. (2011) were adjusted to the Bolfan-Casanova et al. (2018) calibration using a correction factor of 100/55 (Bolfan-Casanova et al., 2018). The error bars for this study and Druzhbin et al. (2021) include the standard deviation of  $C_{H_2O}$  from the multiple spectra, uncertainty of infrared absorption coefficients (Bolfan-Casanova et al., 2018), and uncertainty of the thickness measurements ( $\pm 1 \mu m$ ). The error bars for previous studies are based on their reported values, and with a correction factor of 100/55 if Paterson (1982) calibration was used. The mantle transition zone geotherm at 410–520 km depth is from Katsura et al. (2010), whereas the plume geotherm is assumed to be 200 K higher. FTIR, Fourier transformation infrared spectroscopy.

the Fe-free and Fe-bearing systems (Figure 2a). Therefore, the infrared absorption at  $3,610 \text{ cm}^{-1}$  is likely caused by protons associated with  $Fe^{3+}$  that formed due to the substitution of one  $Si^{4+}$  or two  $Mg^{2+}$  atoms by  $Fe^{3+}$  and  $H^+$ .

### 3.3. $C_{H_2O}$ /Solubility in Fe-Free Wadsleyite

The  $C_{H_2O}$  in the Fe-free wadsleyite show a clear temperature dependence: decreasing from 2.4 wt.% at 1500 K to 0.6 wt.% at 2000 K (Figure 3; Table 1). Because three phases (wadsleyite + enstatite/superhydrous phaseB + melt) coexist in the Fe-free system that has three components ( $MgO + SiO_2 + H_2O$ ), the  $C_{H_2O}$  in wadsleyite should be uniquely constrained at a given pressure and temperature conditions based on the phase rule, and therefore represent the  $H_2O$  solubility despite the variable  $H_2O$  contents in the starting material. The consistency of  $C_{H_2O}$  values in the runs at 17.5 and 21 GPa indicates a relatively small pressure dependence of  $H_2O$  solubility. The  $H_2O$  solubility in Fe-free wadsleyite determined in this study generally agrees with previous results (Bolfan-Casanova et al., 2018; Demouchy et al., 2005; Druzhbin et al., 2021; Inoue et al., 1995; Jacobsen et al., 2005; Litasov et al., 2011) (Figure 3).

### 3.4. $C_{H_2O}$ /Solubility in Fe-Bearing Wadsleyite

Similar to the Fe-free system, the  $C_{H_2O}$  in Fe-bearing wadsleyite also show a negative temperature dependence: decreasing systematically from 2.2 wt.% at 1500 K to 0.65 wt.% at 2100 K, but the temperature dependence is slightly smaller than that in Fe-free wadsleyite (Figure 3). At 1500 K, the  $C_{H_2O}$  values in Fe-free and Fe-bearing wadsleyite are essentially the same. But at 1900–2100 K, the Fe-bearing wadsleyite has clearly

higher  $C_{\text{H}_2\text{O}}$  than the Fe-free samples (Figure 3). The  $C_{\text{H}_2\text{O}}$  of the samples synthesized from Fo90 + 15 wt.%  $\text{H}_2\text{O}$  is within uncertainty identical to that from Fo75 + 15 wt.%  $\text{H}_2\text{O}$  (Figure 3).

The  $C_{\text{H}_2\text{O}}$  in Fe-bearing wadsleyite measured in this study is higher than the values reported by Bolfan-Casanova et al. (2018). Note that the  $\text{H}_2\text{O}$  content in the starting material in Bolfan-Casanova et al. (2018) was relatively small ( $\sim 5\%$ ). Since only two or three phases (wadsleyite, melt, enstatite/superhydrous phaseB) coexist in the Fe-bearing system which has four ( $\text{MgO} + \text{SiO}_2 + \text{H}_2\text{O} + \text{FeO}$ ) or five ( $+\text{Fe}_2\text{O}_3$ ) components, the number of phases is smaller than the number of components. Therefore, even though the pressure and temperature are fixed, the  $C_{\text{H}_2\text{O}}$  in the samples are not uniquely constrained and may vary with bulk  $\text{H}_2\text{O}$  content in the starting material. As demonstrated in Fei and Katsura (2020), if the starting material contains insufficient amount of  $\text{H}_2\text{O}$  (e.g., Fo90 + 5 wt.%  $\text{H}_2\text{O}$ ), the  $C_{\text{H}_2\text{O}}$  in the samples may not have reached its maximum (i.e., the solubility). Instead, with 15 wt.%  $\text{H}_2\text{O}$ , the  $C_{\text{H}_2\text{O}}$  is independent from the bulk  $\text{H}_2\text{O}$  content in the starting material and represents the  $\text{H}_2\text{O}$  solubility (Fei & Katsura, 2020).

Sun et al. (2018) reported  $C_{\text{H}_2\text{O}} = 1.0$  wt.% in Fe-bearing wadsleyite synthesized from Fo90 + 10 wt.%  $\text{H}_2\text{O}$  at 1720 K, which is slightly lower than  $C_{\text{H}_2\text{O}}$  determined in this study. Note that the Paterson (1982) calibration was used in Sun et al. (2018), which may underestimate  $C_{\text{H}_2\text{O}}$ . By adjusting their results to a newer calibration using a correction factor of 100/55 given by Bolfan-Casanova et al. (2018), the  $C_{\text{H}_2\text{O}}$  in Sun et al. (2018) becomes 1.7  $\sim$  1.8 wt.%, which is slightly higher than in this study ( $\sim 1.4$  wt.% at 1720 K) (Figure 3). However, this difference could be caused by experimental uncertainties, including the uncertainty of the correction factor between different infrared calibrations, experimental temperature, and FTIR spectra baseline subtraction. Additionally, Kawamoto et al. (1996) reported exceptionally high  $C_{\text{H}_2\text{O}}$  at 1700 K ( $C_{\text{H}_2\text{O}} \approx 3.0$  wt.%), their data points do not show a temperature dependence, which suggests some errors ( $C_{\text{H}_2\text{O}}$  overestimated or temperature overestimated) because  $\text{H}_2\text{O}$  solubility should decrease with increasing temperature (Figure 3).

### 3.5. (Mg + Fe)/Si Ratio in Hydrous Wadsleyite

To confirm the validity, the  $C_{\text{H}_2\text{O}}$  values obtained by FTIR in this study are independently examined by the (Mg + Fe)/Si atomic ratio because protons are primarily incorporated into the Mg sites in wadsleyite and the (Mg + Fe)/Si ratio should therefore decrease with increasing  $C_{\text{H}_2\text{O}}$  (Sano-Furukawa et al., 2011; Smyth, 1987). The (Mg + Fe)/Si ratio determined by EPMA in this study is plotted as a function of  $C_{\text{H}_2\text{O}}$  and compared with previous studies of both Fe-free and Fe-bearing systems (Bolfan-Casanova et al., 2018; Demouchy et al., 2005; Druzhbin et al., 2021; Inoue et al., 1995; Litasov et al., 2011) in Figure 4. Although different analytical methods were used to determine  $C_{\text{H}_2\text{O}}$  in these studies, including FTIR, secondary ion mass spectroscopy (SIMS), and elastic recoil detection analysis (ERDA), the (Mg + Fe)/Si ratios follow the same  $C_{\text{H}_2\text{O}}$ -(Mg + Fe)/Si relation of two protons substituting on one Mg site. This supports the robustness of the  $C_{\text{H}_2\text{O}}$  values determined by FTIR spectroscopy in the present study.

The slopes of the (Mg + Fe)/Si data are slightly steeper than that for pure  $\text{Mg}^{2+} = 2\text{H}^+$  substitution (Figure 4). This difference may be caused by experimental uncertainty (e.g., uncertainty of the infrared absorption coefficients, uncertainty of the FTIR spectra baseline subtraction, and EPMA uncertainty). On the other hand, the (Mg + Fe)/Si ratio in Fe-bearing wadsleyite is slightly higher than the Fe-free samples, which is likely caused by an additional proton incorporation mechanism in Fe-bearing wadsleyite. Because Fe in wadsleyite can be partially ferric (McCammon et al., 2004), substitution mechanisms of  $\text{Fe}^{3+}\text{-H}^+$  exchange on  $\text{Si}^{4+}$  sites may occur in addition to the  $\text{Mg}^{2+} = 2\text{H}^+$  substitution, which will slightly increase the (Mg + Fe)/Si ratio in comparison with the pure  $\text{Mg}^{2+} = 2\text{H}^+$  substitution mechanism.

## 4. Implications for $\text{H}_2\text{O}$ Storage Capacity in the Mantle Transition Zone

Although  $\text{H}_2\text{O}$  solubility in wadsleyite decreases with increasing temperature, Fe-bearing wadsleyite can still contain approximately 1.0 wt.%  $\text{H}_2\text{O}$  in its crystal structure in the upper part of the mantle transition zone corresponding to 410–520 km depth with a geotherm of 1800–1900 K (Figure 3). This value is essentially the same as that of ringwoodite at 520–660 km depth in the lower part of the mantle transition zone with a geotherm of 1900–2000 K (Fei & Katsura, 2020). This implies that the entire mantle transition could be  $\text{H}_2\text{O}$ -rich. Reducing conditions in the Earth's interior (Frost & McCammon, 2008) may limit the  $\text{H}_2\text{O}$

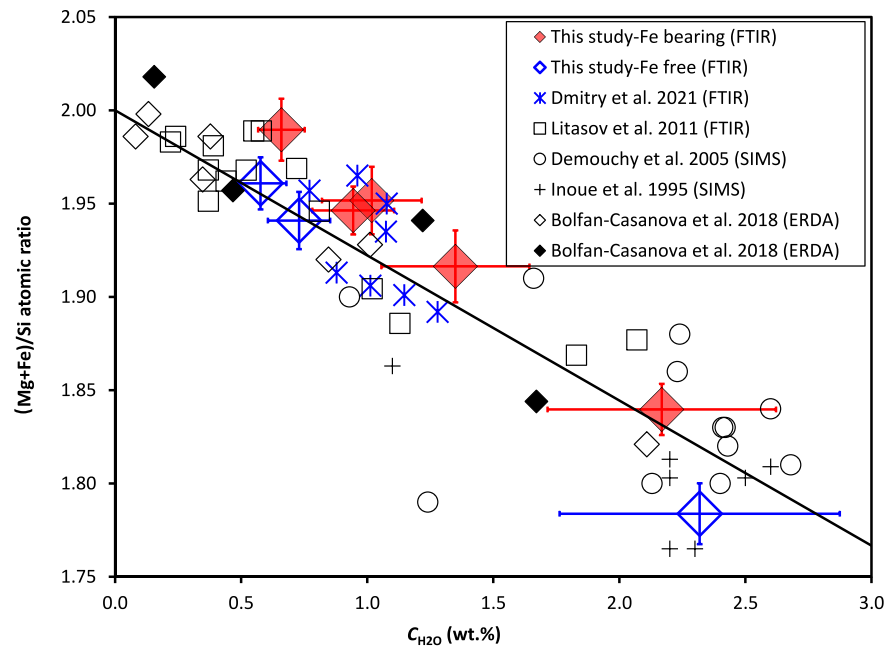


**Figure 4.** (Mg + Fe)/Si ratio as a function of  $C_{H_2O}$ . The solid line is based on the theoretical pure  $Mg^{2+} = 2H^+$  substitution mechanism of protons. The  $C_{H_2O}$  in Litasov et al. (2011) is based on the Paterson (1982) FTIR calibration, which might be underestimated. Filled symbols: Fe-bearing wadsleyite. Unfilled symbols: Fe-free wadsleyite. FTIR, Fourier transformation infrared spectroscopy.

content in some minerals (e.g., Yang et al., 2016; Zhu et al., 2019), however, such limitation may not occur in the mantle transition zone because  $H_2O$  dissociation is negligible in the stabilized wadsleyite field as demonstrated by Druzhbin et al. (2021). A  $H_2O$ -rich mantle transition zone is therefore compatible with low oxygen fugacity and high temperature conditions. This agrees well with previous predications of a  $H_2O$ -rich mantle transition zone (e.g., Fei et al., 2017) and findings of naturally formed  $H_2O$ -rich ringwoodite and ice-VII inclusions (Pearson et al., 2014; Tschauner et al., 2018).

In the case of mantle plumes where temperatures are approximately 200 K higher ( $\sim 2100$  K at 520-km depth) than the ambient mantle, the  $H_2O$  solubility in Fe-bearing wadsleyite is approximately 0.65 wt.%. On the other hand, 1.0 wt.%  $H_2O$  can be dissolved in Fe-bearing ringwoodite at 2100 K (Figure 3). If ringwoodite in the lower part of the mantle transition zone is nearly  $H_2O$ -saturated (Fei et al., 2017), dehydration melting should occur at the 520-km discontinuity caused by the phase transformation from ringwoodite to wadsleyite under  $H_2O$ -saturated conditions driven by upwelling flow in mantle plumes. By assuming 1.0 wt.%  $H_2O$  in ringwoodite (Fei & Katsura, 2020), 0.65 wt.%  $H_2O$  in wadsleyite (this study), a  $H_2O$  content of  $\sim 16\%$  in hydrous silicate melt at 2100 K (Fei, 2021), and a ringwoodite or wadsleyite volume fraction of  $\sim 55\%$  (Frost, 2008), a mass balance calculation indicates a melt fraction of 1.2 vol.% in the dehydration melting layer. Such a high fraction is sufficient to completely wet the grain boundaries of wadsleyite and thus reduce its viscosity and seismic velocity. Therefore, in addition to previously reported dehydration melting layers at the 410- and 660-km discontinuities (Revenaugh & Sipkin, 1994; Schmandt et al., 2014; Vinnik & Farra, 2007), it is predicted that the 520-km discontinuity is also associated with the low velocities and low viscosities near plumes, although the thickness of the dehydration melting layer might be small, and significant amounts of  $H_2O$  are already extracted by plume upwelling, thus seismically difficult to image.

### Data Availability Statement

The FTIR and EPMA data are available in Zenodo (<https://doi.org/10.5281/zenodo.4670183>).

**Acknowledgments**

The authors appreciate Heinz Fischer for high-pressure cell assembly preparation, Detlef Krauß for assistance in EPMA analysis, and Raphael Njul for sample polishing. This work is supported by the Deutsche Forschungsgemeinschaft funding to T. Katsura (KA3434/11-1 and KA3434/12-1) and the annual budget of the Bayerisches Geoinstitut to H. Fei.

**References**

- Bolfan-Casanova, N., Schiavi, F., Novella, D., Bureau, H., Raepsaet, C., Khodja, H., & Demouchy, S. (2018). Examination of water quantification and incorporation in transition zone minerals: Wadsleyite, ringwoodite and phase D using ERDA (Elastic Recoil Detection Analysis). *Frontiers of Earth Science*, 6, 75. <https://doi.org/10.3389/feart.2018.00075>
- Buchen, J., Marquardt, H., Speziale, S., Kawazoe, T., Boffa Ballaran, T., & Kurnosov, A. (2018). High-pressure single-crystal elasticity of wadsleyite and the seismic signature of water in the shallow transition zone. *Earth and Planetary Science Letters*, 498, 77–87. <https://doi.org/10.1016/j.epsl.2018.06.027>
- Chen, J., Inoue, T., Yurimoto, H., & Weidner, D. J. (2002). Effect of water on olivine-wadsleyite phase boundary in the (Mg, Fe)<sub>2</sub>SiO<sub>4</sub> system. *Geophysical Research Letters*, 29, 22–31. <https://doi.org/10.1029/2001GL014429>
- Dai, L., & Karato, S.-i. (2009). Electrical conductivity of wadsleyite at high temperatures and high pressures. *Earth and Planetary Science Letters*, 287, 277–283. <https://doi.org/10.1016/j.epsl.2009.08.012>
- Demouchy, S., Delouie, E., Frost, D. J., & Keppeler, H. (2005). Pressure and temperature-dependence of water solubility in Fe-free wadsleyite. *American Mineralogist*, 90, 1084–1091. <https://doi.org/10.2138/am.2005.1751>
- Demouchy, S., Mainprice, D., Tommasi, A., Couvy, H., Barou, F., Frost, D. J., & Cordier, P. (2011). Forsterite to wadsleyite phase transformation under shear stress and consequences for the Earth's mantle transition zone. *Physics of the Earth and Planetary Interiors*, 184, 91–104. <https://doi.org/10.1016/j.pepi.2010.11.001>
- Deon, F., Koch-Müller, M., Rhede, D., Gottschalk, M., Wirth, R., & Thomas, S.-M. (2010). Location and quantification of hydroxyl in wadsleyite: New insights. *American Mineralogist*, 95, 312–322. <https://doi.org/10.2138/am.2010.3267>
- Druzhbin, D., Fei, H., & Katsura, T. (2021). Independent hydrogen incorporation in wadsleyite from oxygen fugacity and non-dissociation of H<sub>2</sub>O in the reducing mantle transition zone. *Earth and Planetary Science Letters*, 557, 116755. <https://doi.org/10.1016/j.epsl.2021.116755>
- Fei, H. (2021). Water content of the dehydration melting layer in the topmost lower mantle. *Geophysical Research Letters*, 48, e2020GL090973. <https://doi.org/10.1029/2020GL090973>
- Fei, H., & Katsura, T. (2020). High water solubility of ringwoodite at mantle transition zone temperature. *Earth and Planetary Science Letters*, 531, 115987. <https://doi.org/10.1016/j.epsl.2019.115987>
- Fei, H., Yamazaki, D., Sakurai, M., Miyajima, N., Ohfuji, H., Katsura, T., & Yamamoto, T. (2017). A nearly water-saturated mantle transition zone inferred from mineral viscosity. *Science Advances*, 3, e1603024. <https://doi.org/10.1126/sciadv.1603024>
- Frost, D. J. (2003). The structure and sharpness of (Mg,Fe)<sub>2</sub>SiO<sub>4</sub> phase transformations in the transition zone. *Earth and Planetary Science Letters*, 216, 313–328. [https://doi.org/10.1016/s0012-821x\(03\)00533-8](https://doi.org/10.1016/s0012-821x(03)00533-8)
- Frost, D. J. (2008). The upper mantle and transition zone. *Elements*, 4, 171–176. <https://doi.org/10.2113/gselements.4.3.171>
- Frost, D. J., & McCammon, C. A. (2008). The redox state of earth's mantle. *Annual Review of Earth and Planetary Sciences*, 36, 389–420. <https://doi.org/10.1146/annurev.earth.36.031207.124322>
- Hirschmann, M. M., Aubaud, C., & Withers, A. C. (2005). Storage capacity of H<sub>2</sub>O in nominally anhydrous minerals in the upper mantle. *Earth and Planetary Science Letters*, 236, 167–181. <https://doi.org/10.1016/j.epsl.2005.04.022>
- Inoue, T., Yurimoto, H., & Kudoh, Y. (1995). Hydrous modified spinel, Mg<sub>1.75</sub>SiH<sub>0.5</sub>O<sub>4</sub>: A new water reservoir in the mantle transition region. *Geophysical Research Letters*, 22, 117–120. <https://doi.org/10.1029/94gl02965>
- Jacobsen, S. D., Demouchy, S., Frost, D. J., Ballaran, T. B., & Kung, J. (2005). A systematic study of OH in hydrous wadsleyite from polarized FTIR spectroscopy and single-crystal X-ray diffraction: Oxygen sites for hydrogen storage in Earth's interior. *American Mineralogist*, 90, 61–70. <https://doi.org/10.2138/am.2005.1624>
- Katsura, T., & Ito, E. (1989). The system Mg<sub>2</sub>SiO<sub>4</sub>-Fe<sub>2</sub>SiO<sub>4</sub> at high pressures and temperatures: Precise determination of stabilities of olivine, modified spinel, and spinel. *Journal of Geophysical Research*, 94, 15663–15670. <https://doi.org/10.1029/jb094i11p15663>
- Katsura, T., Yoneda, A., Yamazaki, D., Yoshino, T., & Ito, E. (2010). Adiabatic temperature profile in the mantle. *Physics of the Earth and Planetary Interiors*, 183, 212–218. <https://doi.org/10.1016/j.pepi.2010.07.001>
- Kawamoto, T., Hervig, R. L., & Holloway, J. R. (1996). Experimental evidence for a hydrous transition zone in the early Earth's mantle. *Earth and Planetary Science Letters*, 142, 587–592. [https://doi.org/10.1016/0012-821x\(96\)00113-6](https://doi.org/10.1016/0012-821x(96)00113-6)
- Kohlstedt, D. L., Keppeler, H., & Rubie, D. C. (1996). Solubility of water in the  $\alpha$ ,  $\beta$  and  $\gamma$  phases of (Mg, Fe)<sub>2</sub>SiO<sub>4</sub>. *Contributions to Mineralogy and Petrology*, 123, 345–357. <https://doi.org/10.1007/s004100050161>
- Litasov, K. D., Shatskiy, A., Ohtani, E., & Katsura, T. (2011). Systematic study of hydrogen incorporation into Fe-free wadsleyite. *Physics and Chemistry of Minerals*, 38, 75–84. <https://doi.org/10.1007/s00269-010-0382-3>
- Liu, H., & Yang, X. (2020). Solubility of hydroxyl groups in pyroxenes: Effect of oxygen fugacity at 0.2–3 GPa and 800–1200°C. *Geochimica et Cosmochimica Acta*, 286, 355–379. <https://doi.org/10.1016/j.gca.2020.07.034>
- Manthilake, M. A. G. M., Matsuzaki, T., Yoshino, T., Yamashita, S., Ito, E., & Katsura, T. (2009). Electrical conductivity of wadsleyite as a function of temperature and water content. *Physics of the Earth and Planetary Interiors*, 174, 10–18. <https://doi.org/10.1016/j.pepi.2008.06.001>
- McCammon, C. A., Frost, D. J., Smyth, J. R., Laustsen, H. M. S., Kawamoto, T., Ross, N. L., & van Aken, P. A. (2004). Oxidation state of iron in hydrous mantle phases: Implications for subduction and mantle oxygen fugacity. *Physics of the Earth and Planetary Interiors*, 143–144, 157–169. <https://doi.org/10.1016/j.pepi.2003.08.009>
- Mrosko, M., Lenz, S., McCammon, C. A., Taran, M., Wirth, R., & Koch-Müller, M. (2013). Hydrogen incorporation and the oxidation state of iron in ringwoodite: A spectroscopic study. *American Mineralogist*, 98, 629–636. <https://doi.org/10.2138/am.2013.4245>
- Paterson, M. S. (1982). The determination of hydroxyl by infrared absorption in quartz, silicate glasses and similar materials. *Bulletin de Minéralogie*, 105, 20–29. <https://doi.org/10.3406/bulmi.1982.7582>
- Pearson, D. G., Brenker, F. E., Nestola, F., McNeill, J., Nasdala, L., Hutchison, M. T., et al. (2014). Hydrous mantle transition zone indicated by ringwoodite included within diamond. *Nature*, 507, 221–224. <https://doi.org/10.1038/nature13080>
- Revenaugh, J., & Sipkin, S. A. (1994). Seismic evidence for silicate melt atop the 410-km mantle discontinuity. *Nature*, 369, 474–476. <https://doi.org/10.1038/369474a0>
- Sano-Furukawa, A., Kuribayashi, T., Komatsu, K., Yagi, T., & Ohtani, E. (2011). Investigation of hydrogen sites of wadsleyite: A neutron diffraction study. *Physics of the Earth and Planetary Interiors*, 189, 56–62. <https://doi.org/10.1016/j.pepi.2011.07.003>
- Schmandt, B., Jacobsen, S. D., Becker, T. W., Liu, Z., & Dueker, K. G. (2014). Dehydration melting at the top of the lower mantle. *Science*, 344, 1265–1268. <https://doi.org/10.1126/science.1253358>
- Shimajuku, A., Kubo, T., Ohtani, E., Nakamura, T., & Okazaki, R. (2010). Effects of hydrogen and iron on the silicon diffusivity of wadsleyite. *Physics of the Earth and Planetary Interiors*, 183, 175–182. <https://doi.org/10.1016/j.pepi.2010.09.011>
- Smyth, J. R. (1987).  $\beta$ -Mg<sub>2</sub>SiO<sub>4</sub>: A potential host for water in the mantle? *American Mineralogist*, 72, 1051–1055.

- Smyth, J. R. (1994). A crystallographic model for hydrous wadsleyite  $\beta$ - $\text{Mg}_2\text{SiO}_4$ : An ocean in the Earth's interior? *American Mineralogist*, 79, 1021–1024.
- Smyth, J. R., Holl, C. M., Langenhorst, F., Laustsen, H. M. S., Rossman, G. R., Kleppe, A., et al. (2005). Crystal chemistry of wadsleyite II and water in the Earth's interior. *Physics and Chemistry of Minerals*, 31, 691–705. <https://doi.org/10.1007/s00269-004-0431-x>
- Sun, W., Yoshino, T., Sakamoto, N., & Yurimoto, H. (2018). Supercritical fluid in the mantle transition zone deduced from H-D interdiffusion of wadsleyite. *Earth and Planetary Science Letters*, 484, 309–317. <https://doi.org/10.1016/j.epsl.2017.12.032>
- Tschauner, O., Huang, S., Greenberg, E., Prakapenka, V. B., Ma, C., Rossman, G. R., et al. (2018). Ice-VII inclusions in diamonds: Evidence for aqueous fluid in Earth's deep mantle. *Science*, 359, 1136–1139. <https://doi.org/10.1126/science.aao3030>
- Vinnik, L., & Farra, V. (2007). Low S velocity atop the 410-km discontinuity and mantle plumes. *Earth and Planetary Science Letters*, 262, 398–412. <https://doi.org/10.1016/j.epsl.2007.07.051>
- Yang, X. (2016). Effect of oxygen fugacity on OH dissolution in olivine under peridotite-saturated conditions: An experimental study at 1.5–7 GPa and 1100–1300°C. *Geochimica et Cosmochimica Acta*, 173, 319–336. <https://doi.org/10.1016/j.gca.2015.11.007>
- Yoshino, T., & Katsura, T. (2013). Electrical conductivity of mantle minerals: Role of water in conductivity anomalies. *Annual Review of Earth and Planetary Sciences*, 41, 605–628. <https://doi.org/10.1146/annurev-earth-050212-124022>
- Yoshino, T., Manthilake, G., Matsuzaki, T., & Katsura, T. (2008). Dry mantle transition zone inferred from the conductivity of wadsleyite and ringwoodite. *Nature*, 451, 326–329. <https://doi.org/10.1038/nature06427>
- Zhang, B., & Xia, Q. (2021). Influence of water on the physical properties of olivine, wadsleyite, and ringwoodite. *European Journal of Mineralogy*, 33, 1–37. <https://doi.org/10.5194/ejm-33-39-2021>
- Zhang, B., Zhao, C., & Yoshino, T. (2021). Fe–Mg interdiffusion in wadsleyite and implications for water content of the transition zone. *Earth and Planetary Science Letters*, 554, 116672. <https://doi.org/10.1016/j.epsl.2020.116672>
- Zhu, F., Li, J., Liu, J., Dong, J., & Liu, Z. (2019). Metallic iron limits silicate hydration in Earth's transition zone. *Proceedings of the National Academy of Sciences of the United States of America*, 116, 22526–22530. <https://doi.org/10.1073/pnas.1908716116>